THE ASTROPHYSICAL JOURNAL, 251:695–712, 1981 December 15

DIRECTIONALITY EFFECTS IN THE TRANSFER OF X-RAYS FROM AN ACCRETING MAGNETIZED NEUTRON STAR: BEAM AND PULSE SHAPES

P. MÉSZÁROS[1] AND S. BONAZZOLA[2]
Laboratory for High Energy Astrophysics, NASA Goddard Space Flight Center
Received 1981 February 9; accepted 1981 June 18

ABSTRACT

We discuss the direction-dependent transfer of X-rays in a plane-parallel atmosphere with a strong magnetic field perpendicular to the surface. We present a transfer formalism incorporating the full angular and polarization dependence of the cross sections, including vacuum polarization, for frequencies not too close to the cyclotron resonance. We treat the problem of a slab illuminated from below and of a semi-infinite medium at constant temperature and density and present numerical results for parameters typical of the hot polar caps of accreting magnetized neutron stars. Theoretical beam and X-ray pulse shapes are obtained for various models of X-ray pulsars, and the frequency and phase dependence of the pulse structure is briefly compared with observations.

Subject headings: polarization — radiative transfer — stars: atmospheres — stars: magnetic — X-rays: general

I. INTRODUCTION

The directionality of the radiation emitted from a magnetized atmosphere is an as yet not well understood problem, which has lately become of great interest because of its bearings on the beaming pattern of X-ray pulsars. With the advent of direct measurements of the magnetic field strength via cyclotron line features in several quasi-steady, pulsating X-ray sources (Trümper *et al.* 1978; Wheaton *et al.* 1979; Dennis *et al.* 1980), values of several $\times 10^{12}$ gauss have been now confirmed, which should strongly affect the transport properties of the atmospheres of these objects. Stimulated by these observations, some detailed radiative cross section calculations have also become available (Mészáros and Ventura 1978, 1979; Gnedin, Pavlov, and Shibanov 1978; Ventura 1979; Börner and Mészáros 1979; Bussard 1980; Kirk and Mészáros 1980). These cross sections are strongly frequency and angle dependent. However, radiative transfer calculations used for models of X-ray pulsars have up until now concentrated on the frequency distribution of the radiation, using various angle-averaging schemes (Ventura, Nagel, and Mészáros 1979; Nagel 1980; Bonazzola, Heyvaerts, and Puget 1979; Mészáros, Nagel, and Ventura 1980). The angular structure of a pencil beam was studied with approximate cross sections by Basko and Sunyaev (1975), through Monte Carlo simulations by Yahel (1980), and in the optically thick case by Kanno (1980). In the present paper we set up the transport equations for plane-parallel finite and semi-infinite media, with full consideration of the directionality of the radiation. We have generalized Sobolev's (1963) integral equation treatment to take into account the two normal polarizations of the medium and the angular anisotropy of the scattering and absorption cross sections, which is required for a realistic treatment of the magnetized neutron star atmosphere. Nagel (1981) has also attacked this problem by a different method, based on Feautrier's equations. We have solved here the problem of a finite coherently scattering slab illuminated from behind, with internal sources of emission, and also the problem of the semi-infinite radiating medium for a magnetic field perpendicular to the surface (we discuss the case of the field parallel to the slab elsewhere). This approach is valid both for optically thick or thin situations and allows exact boundary conditions to be applied, namely, zero incoming diffuse radiation at the boundaries. In principle, by including thermal and quantum corrections in the scattering kernel, one could treat changes in frequency as well as direction in each scattering event. A full treatment is, however, bound to be numerically very difficult, and we have made here the simplification of neglecting the frequency changes in order to concentrate on the interplay of the polarization and direction changes. We have used the vacuum-corrected cold plasma normal modes and assumed the electron distribution to be a one-dimensional Maxwellian. For photons near the core of the cyclotron resonance (e.g., Wasserman and Salpeter 1980; Kirk and Mészáros 1980), one would have to include both thermal and incoherence effects and also take into account departures from a Maxwellian distribution (e.g., Langer, McCray, and Baan 1980). Our present calculation, therefore, does not

[1]Also at the University of Maryland. On leave of absence from Max-Planck-Institut für Astrophysik, Garching, West Germany.
[2]NAS/NRC Resident Research Associate. On leave of absence from the Observatoire de Meudon, DAF, Meudon, France.

apply for $\omega \approx \omega_H$. However, over most of the continuum part of the spectrum, on which we here concentrate, we expect that the present simplifying assumptions should be fairly good. These calculations with the magnetic field perpendicular to the free surface provide a model for pencil beam patterns of X-ray pulsars in the continuum region of the spectrum. These beam patterns are then convolved with the rotation of the neutron star, assuming various aspects of the orientation of the magnetic and rotation axes to the line of sight, to give theoretical pulse profiles. An interesting result is that the contribution of the vacuum polarization to the anisotropy is quite strong, especially within $\pm 40\%$ of the cyclotron frequency. Also of interest is the appearance of double-pulse structure, already indicated by Basko and Sunyaev (1975) on the basis of approximate calculations. Triple and double pulses can in fact appear, as the frequency becomes progressively less than the cyclotron frequency, and we discuss a possible method of determining the field strength B using this phenomenon. These calculations also show the presence of phase-dependent energy spectral distributions resembling observed ones. A large variety of pulse profiles can be generated with these very simple atmospheres by varying the density, the optical depth, and the external illumination, so that detailed model fits may be ambiguous, especially if in the future one extends these calculations to inhomogeneous atmospheres. On the other hand, except for the observed asymmetry of some profiles (cf. § V), it appears that these theoretical pulses provide a very flexible tool for fitting many of the major features of observed pulses.

II. NORMAL MODE RADIATIVE TRANSFER

In the case of an isotropic, nonpolarized medium, the problem of the directionality of the radiation in a scattering atmosphere has been discussed in differential equation form by Chandrasekhar (1950) and in integral equation form by Sobolev (1963). We extend here the integral equation formalism to a medium with two normal modes of propagation, with corresponding anisotropic and frequency-dependent scattering and absorption cross sections, and a preferred direction given by the magnetic field. For the conditions in X-ray pulsars, throughout most of the continuum one has $(\omega/c)(n_j - n_k) \gg (\mu_j + \mu_k)/2$, where n_i, μ_i are the refractive indices and absorption coefficients, respectively (e.g., Nagel 1980; Mészáros, Nagel, and Ventura 1980). As shown by Gnedin and Pavlov (1974), this reduces the radiation density matrix to diagonal form, so that one obtains a set of equations involving the normal intensities only. We shall assume a plane-parallel configuration, with a magnetic field B directed perpendicular to the surface, along the z-coordinate. In this case, the two normal intensities I_1 and I_2 (per unit circular frequency ω) depend only on z and θ, the angle between the direction of observation and the field direction (z-axis). We can write

$$\cos\theta \frac{dI_1(z,\Omega)}{dz} = -\alpha_1(\Omega) I_1(z,\Omega) + \varepsilon_1^s(z,\Omega) + \varepsilon_1^*(z,\Omega) + \varepsilon_1^0(\Omega),$$

$$\cos\theta \frac{dI_2(z,\Omega)}{dz} = -\alpha_2(\Omega) I_2(z,\Omega) + \varepsilon_2^s(z,\Omega) + \varepsilon_2^*(z,\Omega) + \varepsilon_2^0(\Omega), \tag{1}$$

where $\alpha_i(\Omega)$ is the extinction (scattering plus absorption) coefficient in cm^{-1} for radiation of polarization i traveling in the solid angle $d\Omega$ around Ω and $\varepsilon_i(\Omega)$ is the emissivity in ergs cm^{-3} s s^{-1} sr for mode i into that solid angle. There is an emissivity term due to internal sources (thermal emission), $\varepsilon_i^0(\Omega)$, another due to external sources (outside illumination), $\varepsilon_i^*(z,\Omega)$, and another due to scattering of diffuse radiation in the medium, $\varepsilon_i^s(z,\Omega)$. We assume the thermal emission and absorption to be independent of z, which is valid for a homogeneous isothermal matter distribution. We find the intensity scattered into $d\Omega$, $\varepsilon_i^s(z,\Omega)$ as follows. The energy of radiation of polarization j coming from $d\Omega'$ which is stopped per unit volume and time is $\alpha_j(\Omega') I_j(z,\Omega')\, d\Omega'$. The energy scattered from mode j into mode i is $\lambda_{ji}(\Omega')\alpha_j(\Omega') I_j(z,\Omega')\, d\Omega'$, where

$$\lambda_{ji}(\Omega') = \sigma_{ji}(\Omega') / \left[\sigma_j(\Omega') + \kappa_j(\Omega')\right] = \sigma_{ji}(\Omega')/\alpha_j(\Omega'), \tag{2a}$$

$$\alpha_j(\Omega') = \sigma_j(\Omega') + \kappa_j(\Omega'), \text{ and} \tag{2b}$$

$$\sigma_j(\Omega') = \sigma_{j1}(\Omega') + \sigma_{j2}(\Omega'), \tag{2c}$$

κ_j and σ_j being the absorption and scattering coefficient (in cm^{-1}) of mode j along Ω'. Out of this energy undergoing the scattering $j \to i$, the amount scattered into $d\Omega$ around Ω is $(1/4\pi)\chi_{ji}(\Omega',\Omega)\, d\Omega \lambda_{ji}(\Omega')\alpha_j(\Omega') I_j(z,\Omega')\, d\Omega'$, where $\chi_{ji}(\Omega',\Omega)/4\pi$ is the scattering indicatrix, defined by

$$\frac{\chi_{ji}(\Omega',\Omega)}{4\pi} = \frac{1}{\sigma_{ji}(\Omega')} \frac{d\sigma_{ji}(\Omega',\Omega)}{d\Omega}. \tag{3}$$

We have then

$$\varepsilon_i^s(z,\Omega)=\lambda_{1i}(\Omega')\alpha_1(\Omega')I_1(z,\Omega')\frac{\chi_{1i}(\Omega',\Omega)}{4\pi}+\lambda_{2i}(\Omega')\alpha_2(\Omega')I_2(z,\Omega')\frac{\chi_{2i}(\Omega',\Omega)}{4\pi} \tag{4}$$

$$=I_1(z,\Omega')\frac{d\sigma_{1i}(\Omega',\Omega)}{d\Omega}+I_2(z,\Omega)\frac{d\sigma_{2i}(\Omega',\Omega)}{d\Omega}.$$

For the emissivity due to external illumination we denote the external radiation in the direction Ω_0 incident upon the free surface at $z=0$ by $I_i^*(\Omega_0)$. At a depth z, this gives rise to a diffused emission in the direction Ω equivalent to

$$\varepsilon_i^*(z,\Omega)=I_1^*(\Omega_0)e^{-\alpha_1(\Omega_0)z/\cos\theta_0}\frac{d\sigma_{1i}(\Omega_0,\Omega)}{d\Omega}+I_2^*(\Omega_0)e^{-\alpha_2(\Omega_0)z/\cos\theta_0}\frac{d\sigma_{2i}(\Omega_0,\Omega)}{d\Omega}. \tag{5}$$

Defining the source functions

$$B_i^n(\Omega)=\varepsilon_i^n(\Omega)/\alpha_i(\Omega), \tag{6}$$

where the superscript n stands for s, *, or 0, we can rewrite the system (1) as

$$\frac{\cos\theta}{\alpha_1(\Omega)}\frac{dI_1(z,\Omega)}{dz}=-I_1(z,\Omega)+B_1(z,\Omega),$$

$$\frac{\cos\theta}{\alpha_2(\Omega)}\frac{dI_2(z,\Omega)}{dz}=-I_2(z,\Omega)+B_2(z,\Omega), \tag{7}$$

where

$$B_i(z,\Omega)=B_i^s(z,\Omega)+B_i^*(z,\Omega)+B_i^0(\Omega). \tag{8}$$

The formal solution of equation (7) is then

$$I_i(z,\Omega)=\alpha_i(\Omega)\int_{z_m}^{z}B_i(z',\Omega)e^{-\alpha_i(\Omega)(z-z')/\cos\theta}\frac{dz'}{\cos\theta}, \tag{9}$$

where z_m is a constant determined from the boundary conditions. For these, we assume a slab configuration of width z_0 satisfying

$$I_i(0,\Omega)=0, \quad \text{for } \theta<\pi/2,$$

$$I_i(z_0,\Omega)=0, \quad \text{for } \theta>\pi/2; \tag{10}$$

that is, no incoming diffuse radiation at $z=0$ and $z=z_0$ (I_i denotes the diffuse component only, the direct illumination from outside being I_i^*). It follows that in equation (9) we must set $z_m=0$ for $\theta<\pi/2$ and $z_m=z_0$ for $\theta>\pi/2$. Replacing equation (9) into equations (4), (6), and (8) we obtain the integral equation for B_i:

$$B_i(z,\Omega)=\int d\Omega'\left[\frac{I_1(z,\Omega')}{\alpha_i(\Omega)}\frac{d\sigma_{1i}(\Omega',\Omega)}{d\Omega}+\frac{I_2(z,\Omega')}{\alpha_i(\Omega)}\frac{d\sigma_{2i}(\Omega',\Omega)}{d\Omega}\right]+B_i^*(z,\Omega)+B_i^0(\Omega). \tag{11}$$

Written out in full, with account of the boundary condition (10), this is

$$B_i(z,\Omega)=\sum_{j=1}^{2}\int_0^{2\pi}d\phi'\left[\int_0^{\pi/2}\sin\theta'd\theta'\frac{1}{\alpha_i(\Omega)}\frac{d\sigma_{ji}(\Omega',\Omega)}{d\Omega}\int_0^{z}B_j(z',\Omega')e^{-\alpha_j(\Omega')(z-z')/\cos\theta'}\alpha_j\frac{(\Omega')\,dz'}{\cos\theta'}\right.$$

$$\left.-\int_{\pi/2}^{\pi}\sin\theta'\,d\theta'\frac{1}{\alpha_i(\Omega)}\frac{d\sigma_{ji}(\Omega',\Omega)}{d\Omega}\int_z^{z_0}B_j(z',\Omega')e^{-\alpha_j(\Omega')(z-z')/\cos\theta}\alpha_j(\Omega')\frac{dz'}{\cos\theta'}\right]$$

$$+B_i^*(z,\Omega)+B_i^0(z,\Omega). \tag{12}$$

The external illumination term for a distribution of angles Ω_0 is, from equation (5),

$$B_i^*(z,\Omega)=\int_0^{2\pi}d\phi_0\int_0^{\pi/2}\sin\theta_0\,d\theta_0\left[\frac{1}{\alpha_i(\Omega)}\frac{d\sigma_{1i}(\Omega_0,\Omega)}{d\Omega}I_1^*(\Omega_0)\,e^{-\alpha_1(\Omega_0)z/\cos\theta_0}\right.$$

$$\left.+\frac{1}{\alpha_i(\Omega)}\frac{d\sigma_{2i}(\Omega_0,\Omega)}{d\Omega}I_2^*(\Omega_0)\,e^{-\alpha_2(\Omega_0)z/\cos\theta_0}\right], \tag{13}$$

while the thermal emission term is

$$B_i^0(\Omega)=\frac{\varepsilon_i(\Omega)}{\sigma_i(\Omega)+\kappa_i(\Omega)}=\frac{P_\omega}{1+\sigma_i(\Omega)/\kappa_i(\Omega)}, \tag{14}$$

with P_ω, the Planck function for one polarization, being

$$P_\omega=(2\pi)^{-3}c^{-2}\hbar\omega^3/\left[\exp\left(\hbar\omega/kT\right)-1\right], \tag{15}$$

where we have assumed implicitly that the electron distribution is a one-dimensional Maxwellian. The total intensity coming out at the other end of the slab ($z=z_0$) is then, from equation (9) and the boundary conditions (10),

$$I_i^T(z_0,\Omega)=\int_0^{z_0}B_i(z',\Omega)\,e^{-\alpha_i(\Omega)(z_0-z')/\cos\theta}\frac{\alpha_i(\Omega)}{\cos\theta}dz'+I_1^*(\Omega)\,e^{-\alpha_i(\Omega)z_0/\cos\theta}, \tag{16}$$

and the intensity reflected at $z=0$ is

$$I_i^R(0,\Omega)=-\int_0^{z_0}B_i(z',\Omega)\,e^{-\alpha_i(\Omega)z'/\cos\theta}\frac{\alpha_i(\Omega)}{\cos\theta}d\Omega'. \tag{17}$$

In equation (16) the first term is $I_i(z_0,\Omega)$, the diffuse forward scattered intensity at z_0, and to make up the observed intensity, the second term representing the diminished incoming flux has to be added.

III. METHOD OF CALCULATION: FINITE SLAB

We shall assume the incoming flux $I_i^*(\Omega_0)=I_i^*(\theta_0)$ to be rotationally symmetric about the field B(z-direction). The integrated cross sections (e.g., Appendix A) are ϕ-independent, $\sigma_1(\Omega)=\sigma_i(\theta)$, while the differential cross sections $d\sigma_{ij}(\Omega'\Omega)/d\Omega$ depend on $\phi-\phi'$. From equation (13), $B_i^*(z,\Omega)$ will therefore not depend on ϕ, and from the iterative construction of $B_i(z,\Omega)$ implicit in equation (12), neither will B_i, $B_i(z,\Omega)=B_i(z,\theta)$. The ϕ-integral equation in equation (12) acts therefore only on $d\sigma_{ij}(\Omega',\Omega)/d\Omega$, leading to

$$B_i(z,u)=\sum_{j=1}^{2}\int_0^1 du'\left[G_{ji}(u',u)\int_0^z B_j(z',u')\,e^{-\alpha_j(u')(z-z')/u'}\frac{\alpha_j(u')\,dz'}{u'}\right.$$

$$\left.+G_{ji}(u',u)\int_z^{z_0}B_j(z',u')\,e^{+\alpha_j(u')(z-z')/u'}\frac{\alpha_j(u')\,dz'}{u'}\right]+B_i^*(z,u)+B_i^0(u), \tag{18}$$

where $u=\cos\theta$. We have defined

$$G_{ij}(u',u)=\int_0^{2\pi}d\phi'\frac{1}{\alpha_j(u)}\frac{d\sigma_{ij}(u',u)}{d\Omega}=\frac{1}{\alpha_j(u)}\frac{d\sigma_{ij}(u',u)}{du}, \tag{19}$$

and for the θ-integrals between $\pi/2$ and π we have performed the change of variable $u'\to -u'$ and used the symmetry properties (e.g., Appendix A)

$$G_{ij}(u',u)=G_{ij}(-u',u),\qquad \sigma_i(-u)=\sigma_i(u),\qquad \alpha_i(-u)=\alpha_i(u). \tag{20}$$

The corresponding B_i^* is

$$B_i^*(z,u)=\int_0^1 du_0\left[G_{1i}(u_0,u)I_1^*(u_0)e^{-\alpha_1(u_0)z/u_0}+G_{2i}(u_0,u)I_2^*(u_0)e^{-\alpha_2(u_0)z/u_0}\right]. \tag{21}$$

We have solved numerically the system of equations (18) under the boundary condition of a given incoming beam $I_i^*(u_0)$ impinging on the slab surface at $z=0$ and obtained the reflected ($z=0, \pi/2<\theta<\pi$) and outcoming ($z=z_0, 0<\theta<\pi/2$) beams $I_i^R(u)$, $I_i^T(u)$ by setting a grid of z, u, and u' values and solving iteratively. Some care must be given to the treatment of the exponential (cf. Appendix B). The nature of the cross sections, as determined in particular by the value of ω/ω_H, the ratio of the frequency to the cyclotron frequency, influences the accuracy of the calculation for any finite grid. For very large optical depths, especially if the cross sections are very different for the two modes as is the case for $\omega/\omega_H \ll 1$, the finite slab numerical solution becomes progressively less accurate, and a different set of equations is more advantageous, as described in the next section.

IV. SEMI-INFINITE MEDIUM

Let us first establish the form of the equilibrium solution at very great optical depths, $\alpha_1 z \gg 1, \alpha_2 z \gg 1$. At these depths, the influence of B_i^* on the solution should be negligible. We notice that the exponential terms will be nonnegligible only for $z-z' \approx u'/\alpha_i(u')$. If the optical depth is large for all u, this means we may set $B(z',u') \approx B(z,u')$ and take it out from under the integral sign in equation (18). This is further justified by the consideration that physically one expects B not to depend on z at great depths. If we take z at some arbitrary point, we may set the upper and lower limits of z' as $\pm\infty$ and write

$$B_1(u)=\int_0^1 du'\left[B_1(u')G_{11}(u',u)\int_{-\infty}^{\infty} e^{-|z-z'|\alpha_1(u')/u'}\frac{\alpha_1(u')}{u'}dz'+B_2(u')G_{21}(u',u)\int_{-\infty}^{\infty} e^{-|z-z'|\alpha_2(u')/u'}\frac{\alpha_2(u')}{u'}dz'\right],$$

$$B_2(u)=\int_0^1 du'\left[B_1(u')G_{12}(u',u)\int_{-\infty}^{\infty} e^{-|z-z'|\alpha_1(u')/u'}\frac{\alpha_1(u')}{u'}dz'+B_2(u')G_{22}(u',u)\int_{-\infty}^{\infty} e^{-|z-z'|\alpha_2(u')/u'}\frac{\alpha_2(u')}{u'}dz'\right], \tag{22}$$

that is,

$$B_1(u)=2\int_0^1 B_1(u')G_{11}(u',u)\,du'+2\int_0^1 B_2(u')G_{21}(u',u)\,du',$$

$$B_2(u)=2\int_0^1 B_1(u')G_{21}(u',u)\,du'+2\int_0^1 B_2(u')G_{22}(u',u)\,du'. \tag{23}$$

We seek the conditions for an isotropic solution, $B_i(u)=\overline{B_i}=$constant. Because of the symmetry properties, $d\sigma_{ii}(u,u')/du'=d\sigma_{ii}(u',u)/du$ and $d\sigma_{ij}(u,u')/du'=d\sigma_{ji}(u',u)/du$ $(i\neq j)$ (cf. Appendix A). We can write

$$\overline{B_1}=\overline{B_1}\,2\int_0^1\frac{1}{\alpha_1(u)}\frac{d\sigma_{11}(u,u')}{du'}du'+\overline{B_2}\,2\int_0^1\frac{1}{\alpha_1(u)}\frac{d\sigma_{12}(u,u')}{du'}du',$$

$$\overline{B_2}=\overline{B_1}\,2\int_0^1\frac{1}{\alpha_2(u)}\frac{d\sigma_{21}(u,u')}{du'}du'+\overline{B_2}\,2\int_0^1\frac{1}{\alpha_2(u)}\frac{d\sigma_{22}(u,u')}{du'}du'. \tag{24}$$

From the definition

$$\sigma_i(u)=\int_{-1}^1 du'\frac{d\sigma_{i1}(u,u')}{du'}+\int_{-1}^1 du'\frac{d\sigma_{i2}(u,u')}{du'} \tag{25}$$

and the fact that $d\sigma_{ij}(u,u')/du'=d\sigma_{ij}(u,-u')/du'$, so that $\int_0^1 du'=(1/2)\int_{-1}^1 du'$ in these integrals, we obtain

$$-\overline{B_1}\int_0^1\frac{1}{\alpha_1(u)}\frac{d\sigma_{12}(u,u')}{du'}du'+\overline{B_2}\int_0^1\frac{1}{\alpha_1(u)}\frac{d\sigma_{12}(u,u')}{du'}du'=0,$$

$$\overline{B_1}\int_0^1\frac{1}{\alpha_2(u)}\frac{d\sigma_{21}(u,u')}{du'}du'+\overline{B_2}\int_0^1\frac{1}{\alpha_2(u)}\frac{d\sigma_{21}(u,u')}{du'}du'=0. \tag{26}$$

In equilibrium therefore we have

$$\overline{B_1} = \overline{B_2}\,,\ \overline{I_1} = \overline{I_2}\,, \tag{27}$$

as one might expect.

Let us seek now approximate expressions for $B_i(u, z)$, valid at large optical depths but not quite as large that it would lead to equation (27). We consider a semi-infinite medium, extending from $z=-\infty$ to $z=+z_0$. The equations are

$$B_i(z,u)=\int_0^1 du' G_{1i}(u',u)\int_{-\infty}^{z_0} dz' \frac{\alpha_1(u')}{u'} B_1(z',u')\, e^{-|z-z'|\alpha_1(u')/u'}$$

$$+\int_0^1 du' G_{2i}(u',u)\int_{-\infty}^{z_0} dz' \frac{\alpha_2(u')}{u'} B_2(z',u')\, e^{-|z-z'|\alpha_2(u')/u'}. \tag{28}$$

At $z=-\infty$, $B_1=\overline{B_1}=\overline{B_2}=B_2$, and we may choose z_0 large enough that at $z=0$ this is still true. This will be the case if for all u we have

$$z_0 \gg \max\,[1/\alpha_i(u)],\ i=1,2. \tag{29}$$

Normalizing to $\overline{B_1}=\overline{B_2}=1$, equation (28) becomes

$$B_i(z,u)=\int_0^1 du'\left[G_{1i}(u',u)\int_0^{z_0} B_1(z',u')\, e^{-|z-z'|\alpha_1(u')/u'}\frac{\alpha_1(u')}{u'}\,dz' + G_{2i}(u',u)\int_0^{z_0} B_2(z',u')\, e^{-|z-z'|\alpha_2(u')/u'}\frac{\alpha_2(u')}{u'}\,dz'\right]$$

$$+\int_0^1 du'\left[G_{1i}(u',u)\, e^{-\alpha_1(u')z/u'} + G_{2i}(u',u)\, e^{-\alpha_2(u')z/u'}\right]. \tag{30}$$

The last term, which comes from the integral between $z=-\infty$ and $z=z_0$ under replacement of z_0 by $+\infty$, plays the role of boundary condition.

V. RESULTS

We have performed calculations for a magnetic field strength of $B=0.1B_c=4.4\times10^{12}$ gauss, perpendicular to the surface of the atmosphere, for finite slabs and for semi-infinite media, with grids in z, u, and u' typically of 30 points each. The densities used reflect the values expected in an accreting X-ray pulsar, varying from 10^{20} to 10^{24} cm^{-3}. However, we are not aiming here at providing a model for any specific source, but rather have in view a study of the properties of the radiative transfer in a general situation involving a magnetic field.

An interesting question is the effect of a magnetized atmosphere in reprocessing the directional distribution of an incident beam of light of arbitrary angular distribution. In Figure 1 we have plotted the shape of the outgoing flux at a photon energy of 10 keV as a function of angle for a slab of density $n=10^{22}$ cm^{-3}, $T=10$ keV, and Thomson optical depth $\tau_T=7$. The curve labeled δ is the outgoing intensity for an incoming beam distribution which is a delta function in angle (actually a step function of width 15^0), centered at $\theta=0^0$ (parallel to the field). The curve labeled "cos" is for an input varying as $\cos\theta$, while curve A is for an isotropic input. The curve B is the outgoing intensity for zero input (i.e., due only the self-emission of the slab, bremsstrahlung modified by scattering). The curve C is for a semi-infinite medium of the same density and temperature. The general effect, of course, is toward a broadening of the incoming beam, which increases with the optical depth of the atmosphere. For an input delta function at $\theta=0°$ an optical depth of $\tau_T=7$ (based on $\sigma_T=6.6\times10^{-25}$ cm^2, not on $\sigma[\theta]$) is, however, not yet enough to smear out the incoming beam entirely. Similarly, a cosine input is modified, but higher optical depths would be required to reproduce an isotropic input. A semi-infinite medium produces a beam similar in shape to the isotropic input in a slab. A self-emitting slab (B) produces a hollow beam, as already pointed out by Basko and Sunyaev (1975), which reflects the structure of the cross sections. If one convolves these beam shapes with the rotation of the neutron star, assuming that both poles emit at the same relative intensity, we obtain the pulse shapes of Figure 2. We have used here as illustration two different choices of aspect angles i_1 (between the line of sight and the spin axis) and i_2 (between the spin axis and $\boldsymbol{B}$), namely

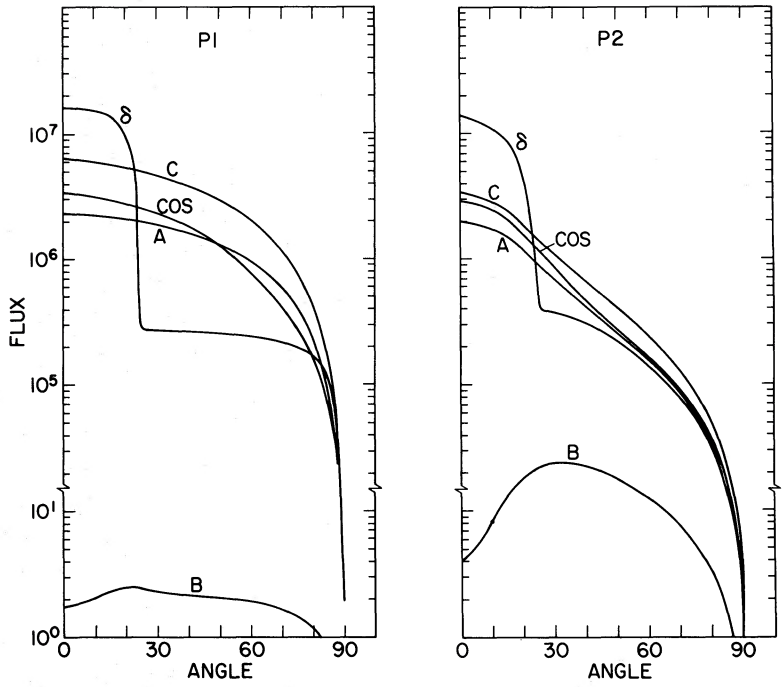

FIG. 1.—Outcoming beam shapes as a function of angle θ for atmospheres of $n=10^{22}$ cm^{-3}, $T=10$ keV. C, semi-infinite atmosphere; B, self-emitting of $\tau_T=7$ and zero external illumination; A, the same with external illumination, isotropically distributed in angle, at blackbody temperature $T_{bb}=5$ keV; cos, same if external illumination is distributed as $\cos\theta$; δ, same if it is distributed as $\delta(\theta)$. (a) Polarization 1, extraordinary; (b) polarization 2, ordinary. The flux is per unit circular frequency ω, i.e., ergs cm^{-2} s^{-1} s.

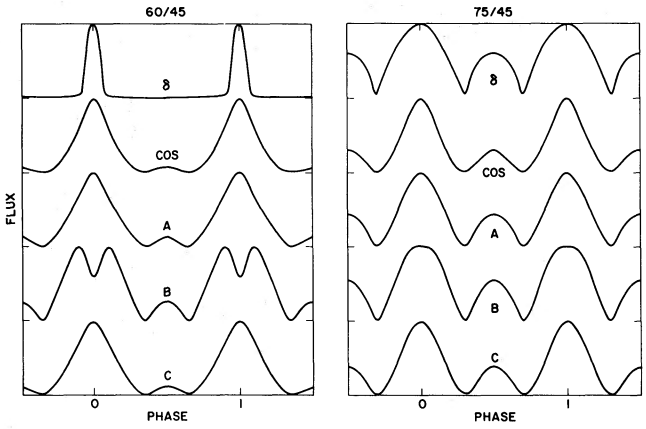

FIG. 2.—Pulse shapes obtained convolving the beam shapes of Fig. 1 with rotation of the neutron star. (a) For inclination angles $i_1, i_2=60°,45°$; (b) for $i_1, i_2=75°,45°$.

$(i_1, i_2)=(60°,45°)$ and $(75°,45°)$. The effective angle θ at which the beam is sampled by the observer is given by

$$\cos\theta=\cos i_1\cos i_2+\sin i_1\sin i_2\cos\phi, \tag{31}$$

where ϕ is the azimuthal angle around B (0 when the beam is pointing closest to the line of sight), and if $\theta>\pi/2$, one takes $\theta\to\pi-\theta$. The profiles are invariant under interchange of i_1 and i_2.

In Figures 3, 4, and 5 we show the outcoming fluxes in both polarizations at photon energies of 1, 10, 20, 30, and 70 keV. The cyclotron frequency is near 50 keV for our field value of $B=0.1B_c$, and in the present paper we avoided this

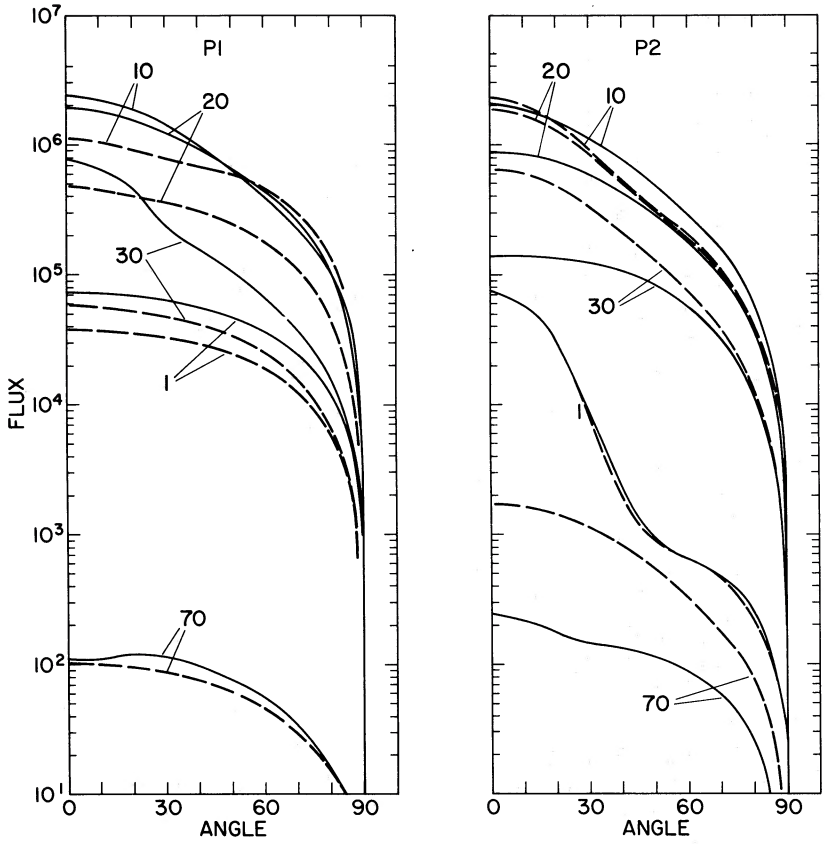

FIG. 3.—Outcoming beam shapes as a function of angle θ for a slab of $\tau_T = 7$, $n = 10^{23}$ cm^{-3}, $T = 10$ keV, $B = 0.1 B_c = 4.4 \times 10^{12}$ gauss ($h\omega_H \approx 50$ keV), photon energies 1, 10, 20, 30, and 70 keV, illuminated by an incoming isotropic beam of blackbody radiation at $T_{bb} = 5$ keV. (*a*) Polarization 1; (*b*) polarization 2. The flux is in ergs cm^{-2} s^{-1} s, the full lines are calculations including vacuum polarization, and the dashed ones are what one would obtain if this is neglected.

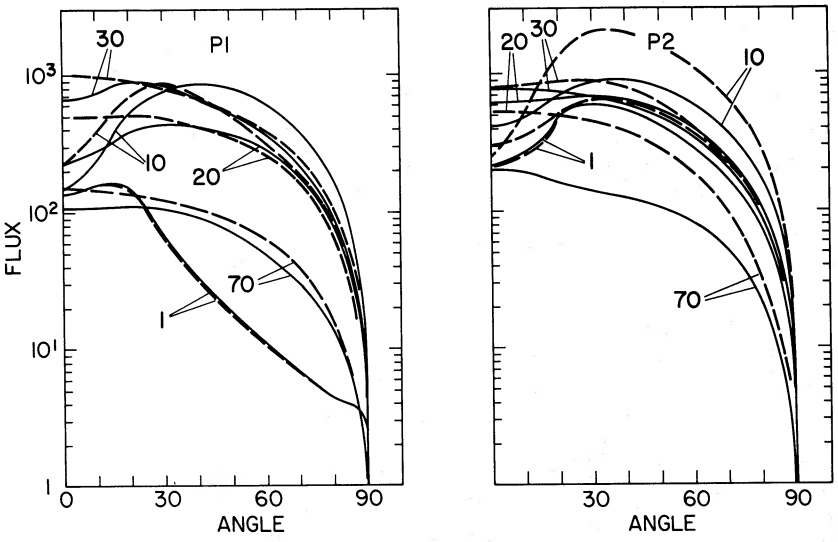

FIG. 4.—Same as Fig. 3, slab of $\tau_T = 7$, but with zero external illumination, self-emission only

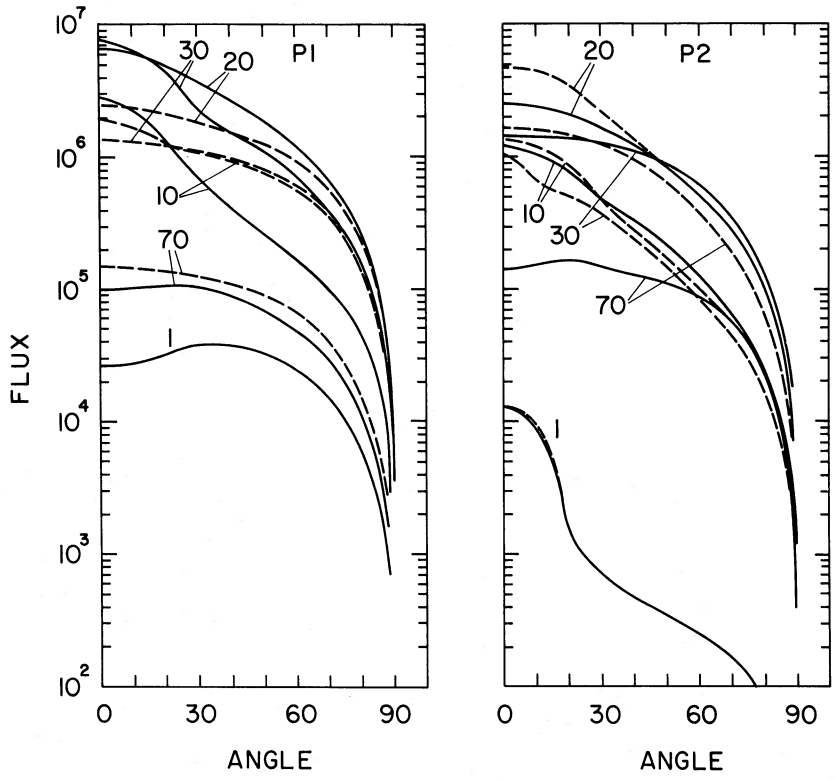

FIG. 5.—Same as Fig. 3, but for a semi-infinite medium

frequency range since to study it properly would require introducing a number of complicating factors (e.g., Kirk and Mészáros 1980). Already for 30 and 70 keV, if the photon propagation angle during its random walk comes close to 0 or π, the photon would have entered the core as defined by Wasserman and Salpeter (1980), so that within the present approximations frequencies closer to ω_H than these could lead to errors. The density and temperature were taken as $n=10^{23}$ cm^{-3} and $T=10$ keV. Figure 3 shows the flux from a slab of $\tau_T=7$ when illuminated by an isotropic blackbody flux ($T_{bb}=5$ keV). Figure 4 is the flux from the same slab when the incoming luminosity is zero (self-radiation only). Figure 5 is the flux from a semi-infinite medium of the same characteristics. These fluxes were computed using the cross sections of Appendix A, the full lines being calculations including vacuum polarization, and the dashed ones neglecting it. One sees that for an external illumination exceeding the luminosity of self-radiation (Fig. 3) the hollow beam structure giving rise to double pulses (visible in Fig. 4) is not present, except to some degree at such frequencies where the background intensity ($T_{bb}=5$ keV) is less than the plasma emission ($T=10$ keV), as is the case at 70 keV for polarization 1 (Fig. 3*a*). It is interesting to compare our Figure 4 with Nagel's (1981) slab results with comparable parameters (his Fig. 7*a*). Some difference is inherent in the fact that we included vacuum polarization, which in Nagel's calculation was set equal to zero, and also his profiles are summed over polarizations and normalized to the blackbody intensity at each frequency. Allowing for this, the two methods seem to lead to fairly similar results. It is also interesting to compare Figure 4 (slab of $\tau_T=7$) and Figure 5 (semi-infinite medium), both without external illumination. As one would expect, the central hollows in the beams tend to fill up as the path length increases.

It is useful also to present beam shapes normalized to unity for singling out the purely angular features, and in Figure 6 we have done this for a semi-infinite medium of $n=8\times10^{23}$ cm^{-3}, $B=0.2B_c$, $T=10$ keV for various values of ω/ω_H, where ω_H in this case is ~100 keV. The full lines are calculations including vacuum polarization, and dashed lines are without. One sees that for a given density and temperature, as one decreases ω/ω_H, the single lobe evolves toward a triple lobe, and as one decreases ω/ω_H even further it becomes eventually a double lobe. Kanno (1980) has computed lobe shapes for the same parameters, using an approximate analytic procedure, which may be compared directly with our Figure 6. It is interesting to see that his approach leads to qualitatively similar predictions concerning the pulse multiplicity, but there are quantitative discrepancies. For instance, for values of $(\omega/\omega_H)^{-1}$ of 20 and 30, with vacuum polarization, Kanno predicts the peak of the sidelobes at $\sim45°$ for both, and normalized intensities of ~0.16 and 0.18, respectively. Our calculation, on the other hand, predicts 38° and 32° with intensities of 0.6 and 0.78,

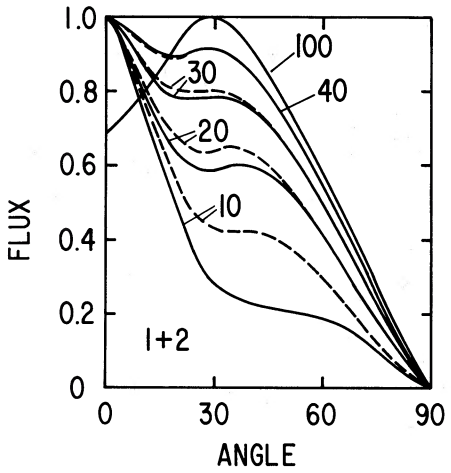

FIG. 6.—Outcoming flux from a semi-infinite medium of $n=8\times10^{23}$ cm^{-3}, $T=10$ keV, and $B=0.2B_c(\hbar\omega_H\approx100$ keV), normalized to unity. Full lines include vacuum, dashed ones do not. The label on the curves is now $(\omega/\omega_H)^{-1}$.

respectively. In general, his method produces rather narrower central lobes than ours, e.g., 8° at intensity 0.5 versus our 19° at 0.5 for $(\omega/\omega_H)^{-1}=10$, and much flatter and less intense sidelobes. A qualitative difference is that we find normalized central lobes which widen with increasing $(\omega/\omega_H)^{-1}$, while Kanno's method gives the opposite behavior, at least for $(\omega/\omega_H)^{-1}=10,20,30$.

While the normalized lobes reveal the angular changes with frequency, the intensity information contained in Figures 3, 4, and 5 is linked with these. The effect of vacuum polarization in the normalized lobe plot of Figure 6 is to narrow the angular distribution and lower the intensity. In the nonrenormalized lobes of Figures 3, 4, and 5 we see, however, that the inclusion of vacuum polarization reshuffles the energy between the frequencies and the polarizations. This is because the radiative cross sections including emission are strongly affected, both in their angular and frequency behavior by the inclusion of the magnetic vacuum polarization (e.g., Mészáros and Ventura 1978, 1979). In the usual plasmas, in the magnetoionic, cold plasma limit, one has negative electrons gyrating all in the same direction and giving rise to predominantly elliptically polarized modes, so that only one mode is resonant, that for which $\boldsymbol{E}$ gyrates in the same sense as the e^-. In the magnetic vacuum of an X-ray pulsar, however, the virtual e^+-e^- pairs can become more important than the real e^-. One has now charges of both signs, almost equal in number and gyrating in opposite directions. This has the effect of driving the normal modes toward becoming nearly linearly polarized, and it also makes the second (ordinary) mode resonant, so that the relative importance of both modes is changed. The cross sections, as seen in Appendix A, are direct functions of the normal polarization vectors and therefore reflect these changes. Although, as discussed for Figure 6, the general effect of the vacuum is to narrow the beam, this appears so because in this plot the flux is normalized. However, the inclusion of the vacuum also alters the relative intensity at a particular frequency because of its effect on the mean free paths and thermalization lengths, etc. This can lead to an increase of intensity at some angles and a decrease at others, e.g., for $\theta<20°$ and $\theta>20°$ at 10 keV in Figure 5*a*, or only to an increase, e.g., 20 keV in the same graph, or only a decrease, e.g., at 70 keV. This naturally shows itself also in the pulse profiles that we discuss further below.

We have plotted in Figure 7 the differential photon energy density u_ω inside the atmosphere as a function of depth z (linear scale) for the individual polarizations and for their sum at a photon energy $\hbar\omega=10$ keV. Curves "*a*" correspond to the slab with background of Figure 3, curves "*c*" to the slab without background of Figure 4, and curves "*b*" to the semi-infinite case of Figure 5. The depth z runs from zero to z_0, and in the slab cases the radiation escapes from both ends, but in "*a*" there is an external illumination incident at $z=0$. The slabs have $\tau_T=7$, while for the semi-infinite case "*b*," the value of z_0 was chosen so as to satisfy the condition (29). For instance, at 10 keV, we took $z_0=1400$ cm or $\tau_T=94$. The number of iterations used for solving the integral equations has to be chosen large enough to ensure that information is propagated across a distance equal to the slab length, or in the semi-infinite medium across a thermalization length. Thus, at 10 keV, where $\sigma_{22}\gg\sigma_{11}\approx\sigma_{12}\approx\sigma_{21}\gg\kappa_2\gg\kappa_1$, for the slab this implies $N_{it}>(\sigma_{12}z_0)^{1/2}$, and for the semi-infinite medium $N_{it}>(\sigma_{12}\kappa_2)^{1/2}$. Typically we used 40 to 60 iterations for the slab models, and over 400 for the semi-infinite models.

We then calculated pulse profiles, shown in Figures 8, 9, and 10, corresponding to the intrinsic beam shapes of Figures 3, 4, and 5, by convolving them with the rotation of the neutron star at different values of the inclination angles i_1 and i_2 of equation (31), indicated at the top of each figure. The total fluxes (1+2) at each frequency (70, 30,

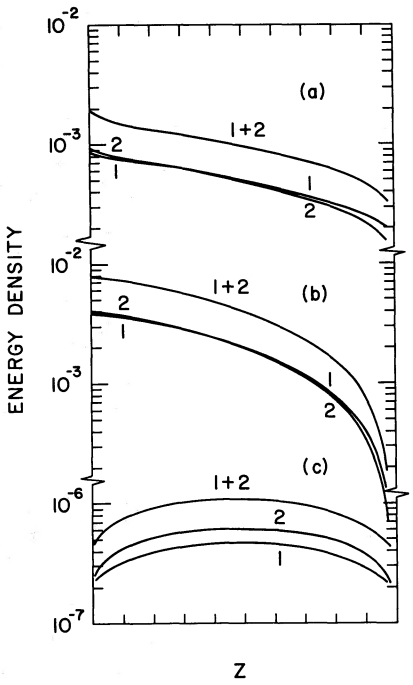

FIG. 7.—Photon energy densities u_ω (ergs cm^{-3} s^{-1}) as a function of depth z at frequency 10 keV, for the slab of Fig. 3 (curve a), the slab of Fig. 4 (curve c), and the semi-infinite medium of Fig. 5 (curve b). Polarizations 1, 2, and their sum 1+2 are given.

20, 10, and 1 keV from top to bottom) were all normalized to unity to emphasize the difference in shape. The full lines are the calculations including vacuum polarization, while the dashed lines are the corresponding calculations without vacuum polarization. It is seen that at most frequencies $\gtrsim$10 keV, the inclusion of vacuum polarization introduces significant differences, and the more so the closer one is to the cyclotron resonance (50 keV for these figures). Depending on the aspect angles i_1, i_2 and the frequency, the pulses can appear broader or narrower than for the zero vacuum case. For the high-intensity cases (slab with background, Fig. 8, and semi-infinite case, Fig. 10) at 10 keV the vacuum narrows the pulse, but in the low-intensity, self-emitting case (Fig. 9) it broadens it. It also changes the depth of the hollow, where present. At 20 and 30 keV, the vacuum in general narrows the pulses, but at some angles this effect reverses. At frequencies larger than the cyclotronic, in general it seems to broaden them, but in practice this is more difficult to observe since the total photon number in the actual observations is lower and the noise higher. These changes introduced by the vacuum polarization reflect the corresponding ones in the cross sections which were discussed previously. The cross sections can become larger at some angles at the expense of other angles, but since the transfer involves a complicated interplay of photon creation, scattering, and polarization exchange, the relative intensities in both polarizations at different frequencies are changed, so that depending on the viewing angles i_1 and i_2 and the phase angle, this can lead to either narrowing or broadening of the pulses.

We have also calculated pulse profiles based on the intrinsic lobes of Figure 6, with $n=8\times10^{23}$ cm^{-3}, $B=0.2B_c$ ($\omega_H=100$ keV), $T=10$ keV, which are shown in Figure 11. The aspect angles i_1, i_2 used were 40/33 and 78/86, and the energy variable was taken to be ω/ω_H, for comparison with Kanno (1980). Our calculation predicts wider central peaks, and the transition to a double peak occurs at lower frequencies than in his approach.

From the point of view of the application to specific models one sees from an examination of the sample of theoretical pulses described above that a broad range of pulse shapes can be reproduced by changing a few basic parameters of even the simplest, uniform atmospheres. One feature observed in many X-ray pulsars is an asymmetry of the pulse shape around phase 0, or 1 (Pravdo *et al.* 1977; Pravdo *et al.* 1979), and this does not appear in our theoretical pulses. One way to reproduce such asymmetries might be to have an inhomogeneous flow along the azimuth of the accretion column. Another possibility would be an asymmetric (nondipole) magnetic field. Without, however, going into the asymmetry, which is not very pronounced in many pulsars, we can attempt a qualitative comparison with some known objects. Two well-studied objects are A0535+26 (Bradt *et al.* 1976) and 3U 0900-40 (McClintock *et al.* 1976). The first shows no interpulse, the main pulse being single at higher energies and splitting into two at lower energies. Looking through Figures 8, 9, 10, and 11 we see that the self-emitting slab of Figure 9 around 50/20, 30/30, or the

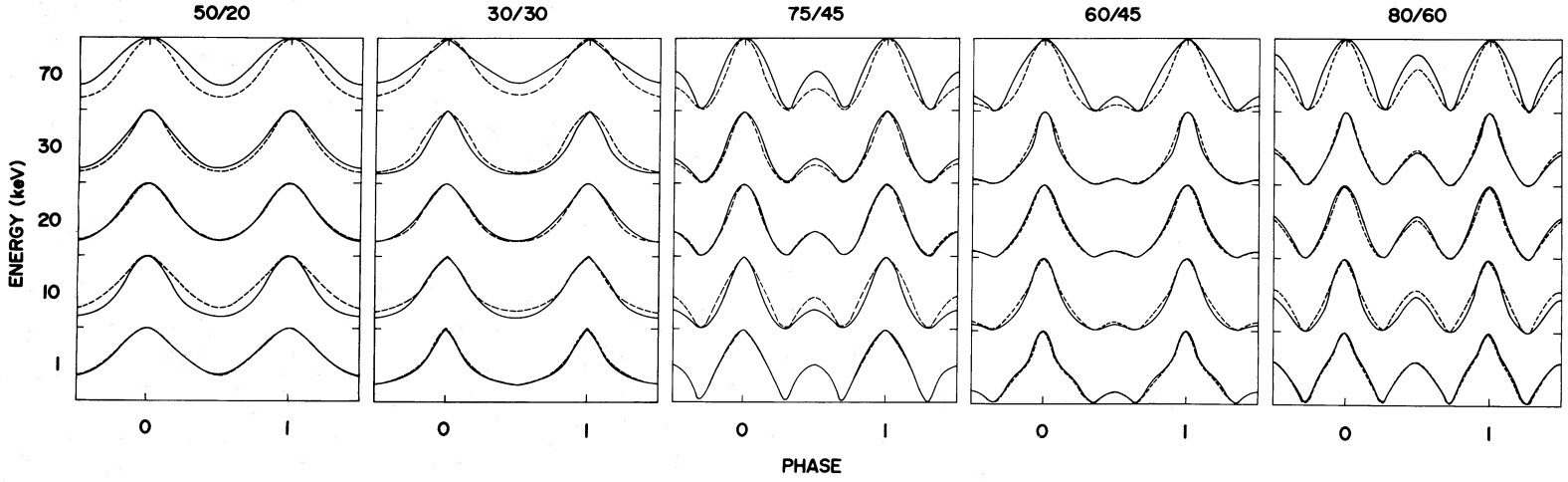

FIG. 8

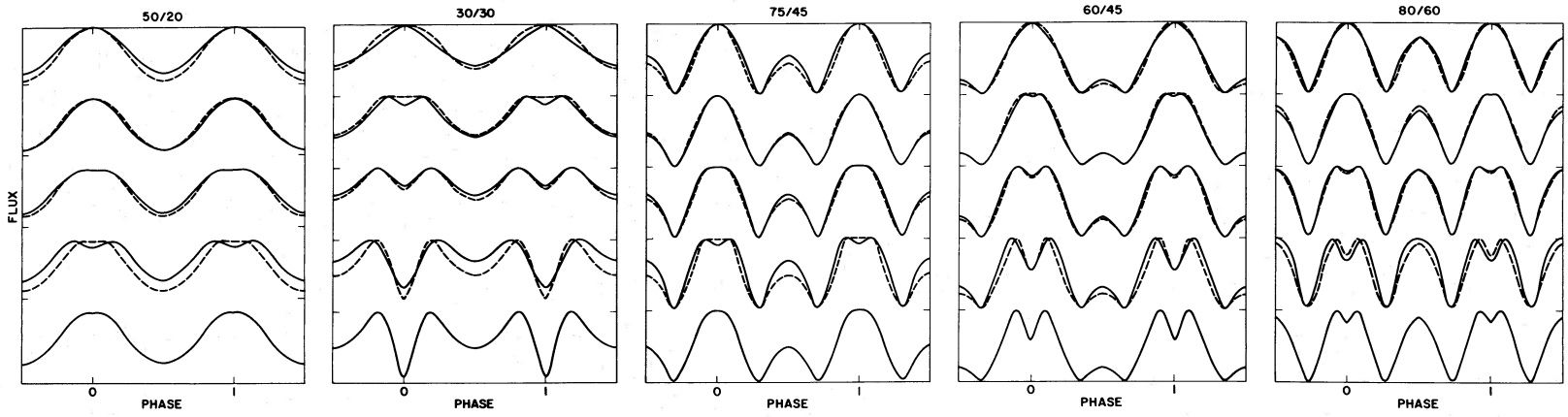

FIG. 9

FIG. 8.—Pulse shapes (polarization 1 and 2 summed) normalized to unit flux for 70, 30, 20, 10, and 1 keV (*top to bottom*) obtained convolving the beam shape of Fig. 3 (slab $\tau_T=7$ with background illumination $T_{bb}=5$ keV) with the rotation of the star, at different values of i_1, i_2, labeled at the top. *Full curves*—including vacuum polarization; *dashed lines*—without it.

FIG. 9.—Same as Fig. 7 for the self-emitting slab of Fig. 4

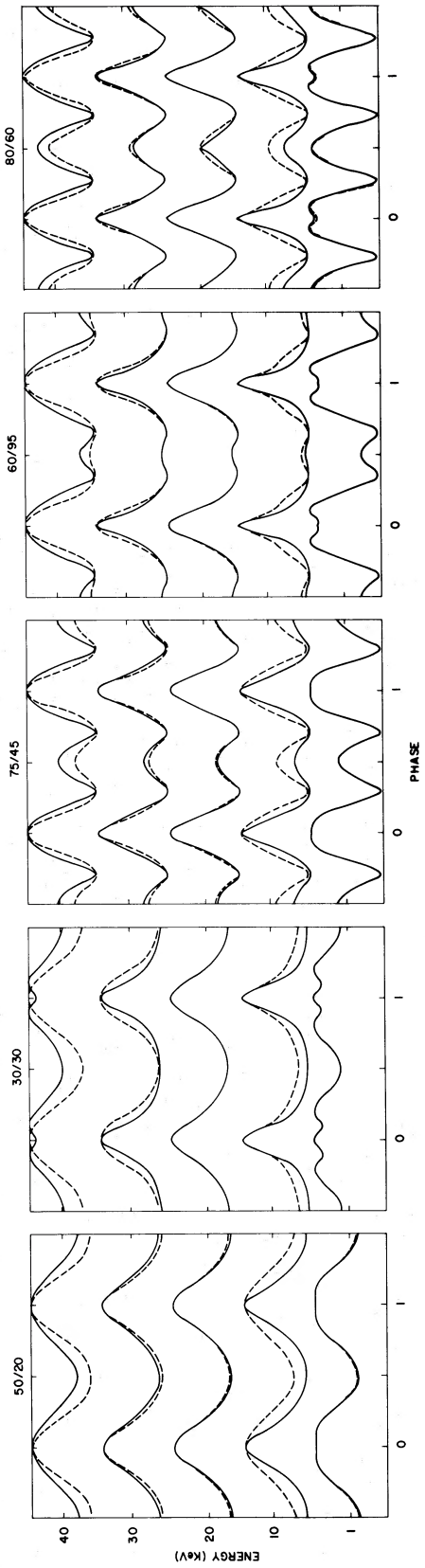

FIG. 10.—Same as Fig. 7, but for the semi-infinite medium of Fig. 5

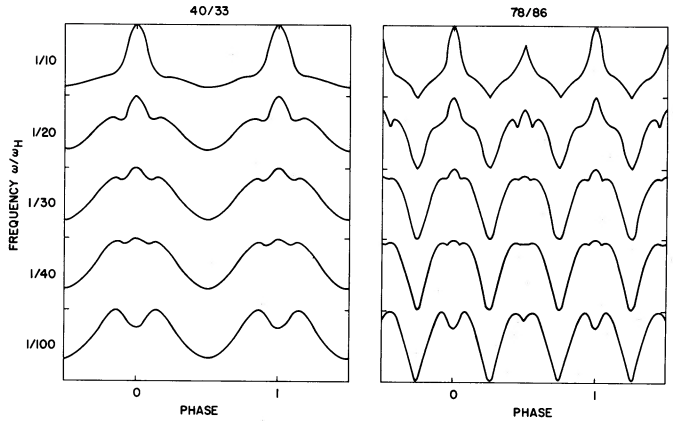

FIG. 11.—Pulse shapes normalized to unit flux for the semi-infinite medium of Fig. 6, for $(\omega/\omega_H)^{-1}=10$, 20, 30, 40, and 100 from top to bottom, and aspect angles of 40/33 and 78/86.

semi-infinite medium of Figure 10 at 30/30 or of Figure 11*a* around 40/33 shows this behavior. In 3U 0900-40 at higher energies there are single main and interpulses, of not too different height, splitting at lower energies into double structures, possibly going through a multiple pulse stage in between. This can be seen in the theoretical profiles of Figure 9, the self-emitting slab at 80/60 or 75/45, and the semi-infinite medium of Figure 10 at 80/60 or of Figure 11*b* at 78/86. Kanno, in fact, suggested on the basis of his approximate calculations semi-infinite atmospheres at 40/33 and 78/86 as possible candidates. It is important to notice that one has the choice of several models, involving different physics. A semi-infinite medium kept at 10 keV is, of course, an idealization in an accreting neutron star. In principle, the heated region should have a depth comparable to the stopping length of incoming protons, which depends on a number of other uncertain variables (whether they are stopped by particle collisions, or if there is a shock, etc.) but perhaps 5–50 g cm^{-2} is the depth of the actual X-ray atmosphere. If the heating is more or less uniform throughout, a self-emitting slab could then be used as a first approximation. On the other hand, if the heating occurs mostly toward the end of the stopping length, a slab with a blackbody illumination from below might serve as approximate model. If downward thermal conduction were very effective, which again is uncertain, a semi-infinite atmosphere might be appropriate. Better (and needless to say more difficult) models would have to consider also density, temperature, and field gradients, as well as departures from plane-parallel symmetry. It is encouraging, however, that even these very simplified models are already able to account for several major features of the observed pulses.

Of potentially great observational interest are the frequency of onset of the multipulse structure and the phase dependence of the energy spectrum. The first of these could, in principle, serve to determine the magnetic field strength, if one did not know it from, say, a cyclotron line measurement. The reason is that for a given density, temperature, and geometry the multipulse behavior sets in at a particular value of ω/ω_H. This method is not applicable, however, to all pulsars, since the aspect angles have to be within a certain range (there are aspect angles at which no multipulse structure shows up). It also makes a difference whether slab or semi-infinite models are used. However, if one is able to adjust the total luminosity by making reasonable guesses for n, T, and z_0, a fit of a particular sequence of pulses at different energies with a theoretical sequence at different ω/ω_H would determine ω_H or B. The other effect is that the spectrum observed varies with phase, as a look at Figures 3, 4, and 5 shows. This effect is known to occur observationally (e.g., Pravdo *et al.* 1977), a hardening of the spectrum occurring toward the middle of the pulse of Her X-1. Without going into details, which would require a number of further considerations, one sees that, for instance, the self-emitting slab of Figure 4 shows a definite hardening toward $\theta=0$, and the semi-infinite model of Figure 5 also has a similar tendency.

To summarize, we have investigated here some of the main properties of the basic radiative transfer in a pencil beam situation. These results give one a feel for the elements one should use in a realistic model of an accretion column, insofar as concerns the structure of the radiation field. It is worth noting that the amount of computation required in this approach is significantly less than in Monte Carlo photon escape calculations. The results discussed here need to be extended to include the fan beam case (field parallel to the free surface; cf. Nagel 1981) and to take account of incoherent scattering, a calculation now in preparation by the present authors. It is clear, in conclusion, that the peculiarities of the cross sections in a magnetic field, as well as the structure of the atmosphere, play a large role in

determining the pulse shapes of accreting neutron stars. Detailed models of astrophysical sources incorporating some of the elements described above should be possible in the near future.

We are grateful to E. Boldt, W. Nagel, R. Ramaty, and the referee for very useful comments.

APPENDIX A

CROSS SECTIONS

We list here the expressions for the cross sections necessary to arrive at the symmetry relationships used in the text (for a discussion see Mészáros and Ventura 1979; Ventura 1979). In this appendix, u is no longer $\cos\theta$ as in the text, standing for a different quantity (cf. eq. [A2]).

The rotating components of the extraordinary (1) and ordinary (2) polarization eigenvectors e^1, e^2 are

$$\begin{aligned} &e^{1,2}=\left(e_z^{1,2}, e_+^{1,2}, e_-^{1,2}\right), \\ &e_z^1=-C\alpha\sin\theta, \qquad e_z^2=-C\sin\theta, \\ &e_+^1=C2^{-1/2}e^{-i\phi}(\alpha\cos\theta+1), \qquad e_+^2=C2^{-1/2}e^{-i\phi}(\cos\theta-\alpha), \\ &e_-^1=C2^{-1/2}e^{+i\phi}(\alpha\cos\theta-1), \qquad e_-^2=C2^{-1/2}e^{+i\phi}(\cos\theta+\alpha), \end{aligned} \tag{A1}$$

where θ is the angle between the magnetic field and the wave vector, ϕ is the axial angle around B, and

$$\begin{aligned} &\alpha\equiv\alpha(\theta)=b\left[1-(1+b^{-2})^{1/2}\right], \qquad C=(1+\alpha^2)^{-1/2}, \\ &b\equiv b(\theta)=2^{-1}(\sin^2\theta/\cos\theta)\,u^{1/2}\left[1+3\delta(1-u)/(uv)\right], \\ &u=(\omega_H/\omega)^2, \qquad v=(\omega_p/\omega)^2, \end{aligned} \tag{A2}$$

where ω_H and ω_p are cyclotron and plasma frequencies. The δ-parameter is the vacuum polarization correction, of value

$$\delta=(45\pi)^{-1}(e^2/\hbar c)(B/B_c)^2\approx 0.5\times 10^{-4}(B/B_c)^2, \tag{A3}$$

where B_c is the critical field $B_c=m^2c^3/e\hbar\approx 4.4\times 10^{13}$ g at which the cyclotron energy $\hbar\omega_H$ equals mc^2.

The differential scattering cross section from mode i at angle θ into mode j at angle θ' is

$$\begin{aligned} \frac{d\sigma_{ij}(\theta,\theta')}{d\Omega'} &= r_0^2\left|e_z^i * e_z^{j'}+\frac{e_+^i * e_+^{j'}}{1+u^{1/2}}+\frac{e_-^i * e_-^{j'}}{1-u^{1/2}}\right|^2 \\ &= r_0^2\left[a_{ij}^2+2a_{ij}(b_{ij}+c_{ij})\cos\beta+(b_{ij}+c_{ij})^2\cos^2\beta+(b_{ij}-c_{ij})^2\sin^2\beta\right], \end{aligned} \tag{A4}$$

where $\beta=\phi'-\phi$, $r_0=e^2/mc^2$,

$$a_{ij}=|e_z^i||e_z^{j'}|, \qquad b_{ij}=|e_+^i||e_+^{j'}|(1+u^{1/2})^{-1}, \qquad c_{ij}=|e_-^i||e_-^{j'}|(1-u^{1/2})^{-1}, \tag{A5}$$

the prime indicating that θ' must be taken. The ϕ-integrated differential cross section is

$$\frac{d\sigma_{ij}(\theta,\theta')}{\sin\theta'\,d\theta'}=\pi r_0^2\left[2a_{ij}^2+(b_{ij}+c_{ij})^2+(b_{ij}-c_{ij})^2\right]=2\pi r_0^2\left[(|e_z^i||e_z^{j'}|)^2+\left(\frac{|e_+^i||e_+^{j'}|}{1+u^{1/2}}\right)^2+\left(\frac{|e_-^i||e_-^{j'}|}{1-u^{1/2}}\right)^2\right], \tag{A6}$$

The integrated polarization exchange cross section is

$$\sigma_{ij}(\theta)=\int_0^{\pi}\frac{d\sigma_{ij}(\theta,\theta')}{\sin\theta'\,d\theta'}\sin\theta'\,d\theta'=\left[A_z^j|e_z^i|^2+\frac{A_+^j|e_+^i|^2}{(1+u^{1/2})^2}+\frac{A_-^j|e_-^i|^2}{(1-u^{1/2})^2}\right], \tag{A7}$$

where $A_\alpha^j=(3/4)\int_{-1}^{1}d(\cos\theta')|e_\alpha^j(\theta',\phi=0)|^2$, and

$$\sum_{j=1}^{2}A_\alpha^j=1. \tag{A8}$$

The integrated cross section summed over outgoing polarizations is

$$\sigma_j=\sigma_{j_1}+\sigma_{j_2}=\sigma_T\left[|e_z^j|^2+\frac{|e_+^j|^2}{(1+u^{1/2})^2}+\frac{|e_-^j|^2}{(1-u^{1/2})^2}\right]. \tag{A9}$$

The free-free absorption cross sections in the limit where one sets Gaunt factors equal to unity (an approximation which should not introduce much greater deviations than some of the other ones made) can be taken as (e.g., Ventura, Nagel, and Mészáros 1979)

$$\kappa_i(\theta)=\sigma_i(\theta)(3\pi/2)\left(Ze^2/\hbar v_{\rm th}\right)\left(n_e c^3/\omega^3\right)(1-e^{-\hbar\omega/kT}), \tag{A10}$$

where $v_{\rm th}=(\pi kT/2m)^{1/2}$ and n_e is electron density.

APPENDIX B

SKETCH OF THE NUMERICAL METHOD

The integrals in equation (18) require some attention to the fact that the kernel $K_i(u)=[\alpha_i(u')/u']e^{\alpha_i(u')(z-z')/u'}$ becomes unwieldy when $\alpha\to\infty$. Let us define

$$\begin{aligned}B_+(J,L)&=\tfrac{1}{2}\left[B(J+1,L)+B(J+1,L)\right],\\ B_-(J,L)&=\tfrac{1}{2}\left[B(J+1,L)-B(J,L)\right],\end{aligned} \tag{B1}$$

where $B(J,L)$ is the value of B computed on the point (J,L) of the integration grid. We have terms of the type

$$\int_0^1 du'G(u',u)\int_0^z B(z',u')\,e^{-(z-z')\alpha(u')/u'}\frac{\alpha(u')\,dz'}{u'}$$

$$=\sum_{L'=0}^{NL-1}\int_{L'k}^{(L'+1)k}du'G(u',u)\sum_{J'=1}^{J-1}\int_{(J'-1)h}^{J'h}B(z',u')\frac{\alpha(u')}{u'}e^{-(z-z')\sigma(u')/u'}dz', \tag{B2}$$

where we have treated for simplicity one polarization only and dropped the index i. Here $h=z_0/(NJ-1)$ is the z-step size, and $k=1/(NL-1)$ is the $u=\cos\theta$ step size, and $J=z/h$. We may assume B and G to be sufficiently smooth that to a good approximation the integral (B2) may be written

$$\int_0^1 du'\cdots\int_0^z dz'\cdots=\frac{1}{4}\sum_{L'=0}^{NL-1}\sum_{J'=1}^{J-1}\Bigg[\left\{G(L'k,u)+G\left[(L'+1)k,u\right]\right\}$$

$$\times\left[B_+(J',L+1)+B_+(J',L)\right]\int_{L'k}^{(L'+1)k}du'\int_{(J'-1)h}^{J'h}\frac{\alpha(u')}{u'}e^{-(z-z')\alpha(u')/u'}dz'\Bigg]. \tag{B3}$$

The double integral becomes

$$\int_{L'k}^{(L'+1)k} du' \int_{(J'-1)h}^{J'h} \frac{\alpha(u')}{u'} e^{-(z-z')\alpha(u')/u'} dz' = \int_{L'k}^{(L'+1)k} \{ e^{-(z-h(J'-1))} - e^{-(z-hJ')} \},$$

and defining the functions

$$\psi_+(J, L) = \int_{k(L-1)}^{kL} e^{-h(J-1)\alpha(u')/u'} du', \tag{B4}$$

the integral (B3) becomes

$$\int_0^1 du' \cdots \int_0^z dz' \cdots = \frac{1}{4} \sum_{L'=1}^{NL-1} \sum_{J'=1}^{J-1} \{ [\{ G(L'k, u) + G[(L'+1)k, u] \} \times [B_+(J', L+1) + B_+(J', L)][\psi_+(J-J', L) - \psi_+(J-J'+1, L)]]. \tag{B5}$$

There is another similar integral, with $z' < z' < z_0$, which analogously becomes

$$\int_0^1 du' \cdots \int_z^{z_0} dz' \cdots = \frac{1}{4} \sum_{L'=1}^{NL-1} \sum_{J'-1}^{NJ-1} [\{ G(kL', u) + G[k(L'+1), u] \} \times [B_+(J', L+1) + B_+(J', L)][\psi_+(J'-J+1, L) + \psi_+(J'-J+2, L)]]. \tag{B5a}$$

The functions $\psi_+(J, L)$ can be computed to the required accuracy and stored at the beginning of the computation. For slabs of $\tau_T \lesssim 3$ this method is accurate to within a few percent.

When the condition $z_0 \alpha(u) \gg 1$ is encountered (too wide a slab, or semi-infinite medium), the above method is no longer adequate. To deal with this case, instead of refining the grid size (which in fact does not help much), it is more advantageous to take into account the effects of the first derivative of B. The integrals (B4), (B5) can be written then as

$$\int_0^1 du' \cdots \int_0^z dz' \cdots = \sum_{L'=1}^{NL-1} \sum_{J'=1}^{J-1} \{ [\hat{B}_+(J', L') + \tfrac{1}{2} \hat{B}_-(J', L')][\psi_+(J-J', L') - \psi_+(J-J'+1, L')] + \hat{B}_-(J', L')[\psi_+(J'-J+1, L') - \psi_-(J'-J, L')] \} \hat{G}(L', u), \tag{B6}$$

where $\hat{B}_\pm(J, L) = (1/2)[B_\pm(J, L) \pm B_\pm(J, L+1)]$, $\hat{G}(J, L) = (1/2)[G_+(J, L) + G(J, L+1)]$, and $\psi_-(J, M) = h^{-1} \int_{M(k-1)}^{Mk} [u/a(u)] e^{-a(u)(J-1)h/u} du$. Similarly,

$$\int_0^1 du' \cdots \int_z^{z_0} dz' \cdots = \sum_{L'=1}^{NL-1} \sum_{J'=J}^{NJ-1} \{ [\hat{B}_+(J', L') + \tfrac{1}{2} \hat{B}_-(J', L')][\psi_+(J'-J+1, L') - \psi_+(J'-J+2, L')] - \hat{B}_-(J', L')[\psi_+(J'-J+1, L') - \psi_-(J'-J+1, L')] \} \hat{G}(L', u). \tag{B7}$$

From the definition of ψ_+, ψ_-, B_+, and B_- one sees that for $\alpha(u) z \gg 1$ the integral (B6) becomes

$$\int_0^1 du' \cdots \int_0^z dz' \cdots = k \sum_{L'=1}^{NL-1} \tfrac{1}{2} [B(J, L') + B(J, L'+1)] G(L', u), \tag{B8}$$

$$\int_0^1 du' \cdots \int_z^{z_0} dz' \cdots = k \sum_{L'=1}^{NL-1} \tfrac{1}{2} [B(J, L') + B(J, L'+1)] G(L', u). \tag{B9}$$

These integrals are the same as one would have in the asymptotic case of equation (23); i.e.,

$$B(J,u)=\int_0^1 G(u',u)B(J,u')\,du'+B^*(J,u), \tag{B10}$$

with an added boundary condition term B^*.

REFERENCES

Basko, M. M., and Sunyaev, R. A. 1975, *Astr. Ap.*, **42**, 311.
Bonazzola, S., Heyvaerts, J., and Puget, J. L. 1979, *Astr. Ap.*, **78**, 53.
Börner, G., and Mészáros, P. 1979, *Plasma Phys.*, **21**, 357.
Bradt, H., *et al.* 1976, *Ap. J.* (*Letters*), **204**, L67.
Bussard, R. W. 1980, *Ap. J.*, **237**, 970.
Chandrasekhar, S. 1960, *Radiative Transfer* (New York: Dover).
Dennis, B. R., Frost, K. J., Kiplinger, A. L., Orwig, L. E., Desai, U., and Cline, T. L. 1980, preprint.
Gnedin, Yu. N., and Pavlov, G. G. 1974, *Soviet Phys.—JETP*, **38**, 903.
Gnedin, Yu. N., Pavlov, G. G., and Shibanov, Yu. A. 1978, *Soviet Astr. Letters*, **4**, 117.
Gruber, D. E., Matteson, J. L., Nolan, P. L., Knight, F. K., Baity, W. A., Rothschild, R. E., and Peterson, L. E. 1980, *Ap. J.* (*Letters*), **240**, L127.
Kanno, S. 1980, *Pub. Astr. Soc. Japan*, **32**, 105.
Kirk, J. G., and Mészáros, P. 1980, *Ap. J.*, **241**, 1153.
Langer, S. H., McCray, R., and Baan, W. A. 1980, *Ap. J.*, **238**, 731.
Mazets, E. P., Golenetskii, S. V., Aptekar', R. L., Guryan, Yu. A., and Il'inskii, V. N. 1981, *Nature*, **282**, 587 preprint.
McClintock, J. E., *et al.* 1976, *Ap. J.* (*Letters*), **206**, L99.
Mészáros, P., Nagel, W., and Ventura, J. 1980, *Ap. J.*, **238**, 1066.
Mészáros, P., and Ventura, J. 1978, *Phys. Rev. Letters*, **41**, 1544.
_____. 1979, *Phys. Rev. D*, **19**, 3365.
Nagel, W. 1980, *Ap. J.*, **236**, 904.
_____. 1981, preprint.
Pravdo, S. H., Boldt, E. A., Holt, S. S., and Serlemitsos, P. J. 1977, *Ap. J.* (*Letters*), **216**, L23.
Pravdo, S. H., *et al.* 1979, *Ap. J.*, **231**, 912.
Sobolev, V. V. 1963, *A Treatise on Radiative Transfer* (Princeton: Van Nostrand).
Trumper, J., Pietsch, W., Reppin, C., Voges, W., Staubert, R., and Kendziorra, E. 1978, *Ap. J.* (*Letters*), **219**, L105.
Ventura, J. 1979, *Phys. Rev. D*, **19**, 1684.
Ventura, J., Nagel, W., and Mészáros, P. 1979, *Ap. J.* (*Letters*), **233**, L125.
Wasserman, I., and Salpeter, E. E. 1980, *Ap. J.*, **241**, 1107.
Wheaton, W. *et al.* 1979, *Nature*, **282**, 240.
Yahel, R. 1980, *Astr. Ap.*, **30**, 26.

Note added in proof.—In Figure 3 the curves are labeled (from top to bottom) 70, 30, 40, 20, 10, 1 keV. In Figure 10, the top label 40 should read 70, and the fourth set of curves should read 60/45.

P. MÉSZÁROS: Laboratory for High Energy Astrophysics, Code 665, NASA Goddard Space Flight Center, Greenbelt, MD 20771

S. BONAZZOLA: DAF, Observatoire de Meudon, 92190 Meudon, France